npg

LABORATORY METHODS

Preclinical animal models of multiple myeloma

Seint T Lwin[1], Claire M Edwards[1,2] and Rebecca Silbermann[3]

[1]Nuffield Department of Surgical Sciences, University of Oxford, Oxford, UK. [2]Nuffield Department of Orthopaedics, Rheumatology and Musculoskeletal Sciences, Botnar Research Centre, University of Oxford, Oxford, UK. [3]Division of Hematology/Oncology, Indiana University School of Medicine, Indianapolis, IN, USA.

Multiple myeloma is an incurable plasma-cell malignancy characterized by osteolytic bone disease and immunosuppression. Murine models of multiple myeloma and myeloma bone disease are critical tools for an improved understanding of the pathogenesis of the disease and the development of novel therapeutic strategies. This review will cover commonly used immunocompetent and xenograft models of myeloma, describing the advantages and disadvantages of each model system. In addition, this review provides detailed protocols for establishing systemic and local models of myeloma using both murine and human myeloma cell lines.

Introduction

Multiple myeloma (MM) is the second most common hematologic malignancy and is characterized by the proliferation of abnormal clonal plasma cells and the production of monoclonal immunoglobulin.[1] Myeloma is the most frequent malignancy to involve the bone, with 80–90% of patients developing bone lesions during the course of their disease, and MM bone disease remains a major source of patient morbidity and mortality.[2] Although therapeutic advances, including the development of novel agents such as immunomodulators (thalidomide, lenalidomide and pomalidomide) and proteasome antagonists (bortezomib, carfilzomib), have markedly improved the overall survival of myeloma patients,[3] MM remains incurable and myeloma bone lesions persist and rarely heal, even in the absence of active disease.

MM develops from the precursor condition monoclonal gammopathy of undetermined significance (MGUS) as a result of the accumulation of oncogenic events, which vary between patients. These mutations include, but are not limited to, hyperdiploidy, primary *IgH* translocations, dysregulation of *cyclin D1*, *MYC* deregulation, chromosome 13 deletions, loss of chromosome 17p, activating mutations of *RAS* or *B-RAF* and secondary translocations.[4] In recent years, it has become clear that an improved understanding of the pathogenesis of myeloma requires consideration of both the genetic abnormalities intrinsic to the malignant myeloma cell and the interactions between myeloma cells and the bone marrow niche (composed of stromal cells, osteoblasts, osteoclasts, endothelial cells, adipocytes and fibroblasts), which are critical for the growth and survival of MM cells. In some cases, however,

myeloma cells can lose their dependence on the bone marrow microenvironment, resulting in the development of extramedullary plasmacytomas (soft tissue plasma-cell tumors) and/or plasma-cell leukemia. These developments represent an aggressive form of myeloma with a poor prognosis.

Murine models of myeloma are critical tools for an improved understanding of the pathogenesis of multiple myeloma, mechanisms of disease resistance and the development of new therapeutic strategies. Although a number of preclinical models of MM and extramedullary plasmacytoma have been described and are commonly used, few adequately model malignant plasma cell–bone marrow microenvironment interactions or allow manipulation of the bone marrow microenvironment. In addition, no single system effectively models either the spectrum of accumulated genetic changes acquired by individuals over the course of their disease or the heterogeneity of disease between individual patients. Therefore, it is imperative that investigators choose the model system most appropriate for their individual research program. For example, an investigator interested in preclinical screening of myeloma compounds will likely choose *in vivo* model systems that are different from an investigator interested in the progression of MGUS to MM. The choice of system will ultimately depend on a number of factors, including the requirement for an intact host immune system, the use of human cell lines or primary human myeloma cells, the extent of osteolytic bone disease that can be induced in the system and the ability to genetically modify the myeloma cells, the host microenvironment or both. In this review, we describe several preclinical immunocompetent and xenograft models of myeloma and provide detailed protocols

Correspondence: Dr R Silbermann, Division of Hematology/Oncology, Indiana University School of Medicine, 980W. Walnut Street, R3 C310, Indianapolis, 46202 IN, USA.
E-mail: rsilberm@iu.edu

for establishing systemic and local disease in the C57BL/KaLwRij 5T Radl, $RAG\text{-}2^{-/-}$ or beige/nude/SCID models of murine myeloma and the Fox Chase SCID model of human myeloma.

Materials and Methods

Protocols for establishing disease in murine model systems must be presented to and approved by institutional animal care committees prior to initiation and should be performed under the supervision of appropriate veterinary staff. Institutional regulations regarding specific procedures, including the frequency and allowable volumes of blood that may be drawn from animals during the course of an experiment, may vary from the guidelines provided here. Suggested protocols described are to be used as guidelines, and modifications may be necessary depending on institutional requirements, models used or experimental questions.

Animal husbandry

1. Maintain mice in pathogen-free animal facility maintained at a constant room temperature with 12-h light and dark cycles.
2. House no more than five mice per cage with regular chow diet and water.
3. Transfer mice to new cages once a week.

Procedure before myeloma cell inoculation

1. Use age-, sex- and weight-matched mice.
2. Earmark and weigh the mice.
3. Perform baseline blood collection per institutional guidelines.
4. Collect blood with BD microtainer serum separator tube.
5. Centrifuge the blood tubes at 6500 r.p.m. for 5 min at 4 °C, and aliquot, and store serum at −80 °C for further analysis.
6. For xenograft models (SCID mice), if required, irradiate animals with a sublethal dose of 300 Rads of total body irradiation 24 h prior to implantation of myeloma cells.

Cell preparation

1. Count murine or human myeloma suspension cells cultured in RPMI 1640 media supplemented with 10% fetal bovine serum, 1% L-glutamine, 1% sodium pyruvate, 1% non-essential amino acid and 1% penicillin/streptomycin.
2. Centrifuge the cells at 2000 r.p.m. for 5 min at room temperature.
3. Resuspend the cells in sterile phosphate-buffered saline (PBS) at 10^7 cells ml^{-1} and place on ice.
4. It is important to inoculate the cells as soon as possible, while the cells are viable.

Inoculation of myeloma cells

Tail vein injection. Tail vein injection is used to induce systemic disease. The rate of tumor engraftment and the proportion of intramedullary to extramedullary tumor that engrafts are dependent on the cell line that is introduced.

1. Transfer the mice to non-sterile procedure room.
2. Place the mouse in a restrainer and stabilize the tail.
3. Gently warm the tail with a heat lamp to help dilate the veins.
4. Clean the tail with an ethanol swab.
5. Mix myeloma cells thoroughly before drawing the cell suspension into the syringe with a needle.
6. Inject 10^6 cells in 100 μl of PBS through the tail vein.
7. Inject 100 μl of PBS for non-tumor control mice.
8. Hold and apply pressure at the injection point for a few seconds to stop the bleeding from the tail.
9. Return the mouse to the cage and monitor for a few minutes.
10. Weigh the mice weekly and monitor them regularly.
11. The mice become paraplegic and develop features of myeloma ∼4 weeks after inoculation.

Subcutaneous injection. Subcutaneous injection over the flank is used to induce solitary plasmacytomas. This is a useful method to determine the rate of tumor growth at extraosseous sites independent of the bone marrow microenvironment.

1. Induce anesthesia.
2. Remove hair from the site of inoculation.
3. Mix myeloma cells thoroughly before drawing the cell suspension into the syringe with a needle.
4. Once the mouse is anesthetized, gently free the skin over the flank from the underlying muscle using a pair of blunt forceps.
5. Inject 10^6 cells in 100 μl of PBS directly beneath the skin over the flank. Subcutaneous injection of human myeloma cells may require matrigel for successful tumor infiltration in xenograft models,[5] whereas murine myeloma cells grow well in C57BL/KaLwRij mice without a requirement for matrigel.[6]
6. Inject 100 μl of PBS for non-tumor control mice.
7. Monitor the mice until they recover from anesthesia.
8. Once tumors are palpable, make serial measurements of tumor diameters daily in three dimensions using electronic calipers.
9. Calculate tumor volumes using the following formula: $4\pi/3 \times (\text{width}/2)^2 \times (\text{length}/2)$.[7]
10. Kill the mice when their tumors reach the diameter stated by individual institutional guidelines.

Intratibial injection. Inoculation of myeloma cells into the cortex of the anterior tuberosity of the tibia, through the tibial plateau, can reliably induce lytic bone lesions in the limb that was directly inoculated. Using this model, little systemic disease is noted outside of the injected limb. In addition, the non-injected (contralateral) limb rarely develops lytic disease and thus can be treated as a control.

1. Anesthetize animals and pre-treat mice with an analgesic of choice prior to injection.
2. Clean legs to be injected with betadine and 70% ethanol. Hair and skin do not need to be removed.
3. Suspend myeloma cells in 20 μl total suspension volume. Inject myeloma cells or saline control into the anterior tuberosity of the tibia with a 27-gauge 0.5-inch needle while flexing the knee. After penetration of the cortical bone, the needle is further inserted into the shaft of the tibia.

4. To prevent leakage of the cells or saline from the injection site, a sterile cotton swab is held against the site for 1 min following removal of the needle.
5. Monitor tumor progression in mice weekly by x-ray, microCT (under isoflurane) and/or fluorescent imaging.

Weekly blood collection

1. Weigh the mice and take blood weekly.
2. Collect ~10 μl (or a volume allowable by institutional guidelines) of the blood with a pipette and transfer to 1.5 ml Eppendorf tubes on ice.
3. Once the blood has clotted, centrifuge the tubes at 6500 r.p.m. for 5 min at 4 °C and collect the sera and store at −80 °C.

Bioimaging

Tumor progression in mice injected with green fluorescent protein (GFP)- or luciferase-tagged myeloma cells can be monitored by *in vivo* fluorescence imaging, bioluminescent imaging or magnetic resonance imaging (MRI).[5,8,9]

Fluorescent imaging

1. Image mice weekly after inoculation of GFP-tagged myeloma cells to assess tumor burden.
2. Anesthetize mice, remove hair and image for GFP signal.
3. Fluorescence imaging can be acquired using Xenogen IVIS Spectrum System (Caliper Life Sciences, PerkinElmer, Waltham, MA, USA), LT-9500 fluorescent light box (Lightools Research, Encinitas, CA, USA), or an Illumatools fiber-optic fluorescence lighting system (Epi model LT-9500; Lightools Research),[8,9] or similar equipment.[5]

Bioluminescence imaging

1. Image mice weekly after inoculation of luciferase-tagged myeloma cells to assess tumor burden.
2. Inject (intraperitoneally) mice with D-luciferin (1.5 mg per mouse, (PerkinElmer)).
3. Image mice 9 min after injection using IVIS or similar equipment.
4. Acquire images by 60 s exposure time or make adjustment to the exposure time depending on the acquired signal.
5. Quantify the intensity of luciferase signal by measuring average radiance (p/s/cm2/sr) using Living Image 4.0 software[5] or similar software (PerkinElmer).

Magnetic resonance imaging

1. Anesthetize and restrain mice.[5]
2. Use a 7T horizontal bore Bruker system or similar equipment to acquire MRI scans.
3. Acquired T2-weighted TurboRARE images using $TE = 24.6$ ms, $TR = 6000$ ms, coronal slice thickness 0.3 mm, FOV 30×30 mm, matrix 100×100, 16 averages and AQ ~14 min.[5]
4. Identify hyperintense signal as tumor enclosed within the cortical bone among T2-weighted images.
5. Draw regions of interest (ROI) in each slice on the periphery of the hyperintense signal in OsiriX and quantified tumor burden from drawn ROI.

Calcein injection to measure bone formation rate

To determine dynamic changes in bone formation, inject mice intraperitoneally with 20 mg kg^{-1} calcein green in PBS (pH 7) ~2 and 6 days prior to experimental end point. Different fluorophores such as calcein green, tetracycline yellow, xylenol orange and alizarin red can also be used to measure bone formation[10] The time between each fluorophore varies depending on the age of the mice used.[11,12] After mice are killed, collect the spines and then fix in 10% neutral-buffered formalin for at least 48 h at 4 °C.

Spine embedding in resin and histology.

1. Process the spines for 1 day each in 70%, 95% and $3 \times 100\%$ ethanol.
2. Place the spines in monomer mix I, II and III at 4 °C in explosion-proof refrigerator for 1–4 days. Make up solution under a fume hood in a darkened bottle.

   Monomer mix I:
   60 ml methyl methacrylate
   35 ml butyl methacrylate
   5 ml methyl benzoate
   1.2 ml polyethylene glycol 400

   Monomer mix II:
   100 ml monomer mix I
   0.5 g wet benzoyl peroxide
   Mix and filter through calcium chloride to remove water. Use a glass funnel lined with gauze to hold in the calcium chloride pellets and pour the solution over the pellets.

   Monomer mix III:
   100 ml monomer mix I
   1 g wet benzoyl peroxide
   Mix and filter through calcium chloride.

3. Make embedding mix just before use and pour quickly, embed the spines in glass scintillation vials and leave the vials in explosion-proof −20 °C freezer for 2–3 days.

   Embedding mix:
   100 ml cold monomer mix III
   400 μl N, N-dimethyl-p-toluidine

4. Once the resin polymerizes, wrap the glass vials well in paper towels and break the vials by hitting gently with the hammer. Wear eye protection.
5. Carefully wash blocks under a running tap.
6. Cut 6-μm thick sections using microtome and view unstained by epifluorescence microscopy and measure bone formation rate by using OsteoMeasure software (Osteometrics, Inc., Decatur, GA, USA).

Culling procedure

1. At the end point of *in vivo* studies, weigh and kill the mice.
2. Immediately collect blood and process as described in the section 'Procedure before myeloma cell inoculation' step 5 to obtain sera.

3. Collect hind legs, spleens and spines.

4. If desired, weigh the spleen and cut a small piece of spleen from myeloma-bearing mice from the same area from each mouse. Obtain splenic cells by homogenization in PBS.

5. Lyse red blood cells for 5 min on ice, using lysis buffer consisting of 155 mM NH_4Cl, 0.1 M KCO_3 and 0.5 M Na_2EDTA.

6. Wash the cells with PBS and fix with 4% formalin overnight at 4 °C.

7. Wash the splenic cells with PBS.

8. Fix the rest of the spleen, spine and one hind leg with the femoral head and end of tibia cut off in 10% formalin.

9. Assess tumor burden in the sera by enzyme-linked immunosorbent assay (ELISA) analysis of the myeloma-specific immunoglobulin IgG2bκ, as developed previously.[13]

10. Filter fixed cells from both bone marrow and spleen through a 70 μm filter (Thermo Scientific, Waltham, MA, USA).

11. Assess tumor burden in spleen by quantitating the percentage of GFP-positive myeloma cells using flow cytometric analysis.

12. Measure myeloma bone disease by microcomputed tomography (μCT), histology and histomorphometric analysis.

Bone marrow isolation by centrifugation

1. After collecting the hind limbs, cut the ends off of the tibia and femur from one limb (**Figure 1**).

2. Place both the tibia and femur in 0.5 ml Eppendorf tubes with open ends at the bottom of the tubes.

3. Cut the lids off of the 0.5 ml Eppendorf tubes.

4. Place Eppendorf tubes with bones in the 1.5 ml Eppendorf tubes with 500 μl of PBS in each tube.

5. Isolate bone marrow by centrifuging mouse tibia and femur at full speed for 2 min (**Figure 1**).

6. Wash bone marrow lysates with PBS.

7. Lyse red blood cells and analyze tumor burden as described in section describing method for Calcein injection, steps 5, 6, 7, 10 and 11.

Assessment of tumor burden by ELISA

1. Coat a high binding ELISA plate (Corning Costar, Fisher Scientific, Pittsburgh, PA, USA) overnight at 4 °C with 2 ug ml^{-1} of antibody appropriate for the cell line used (that is, IgG2bκ capture antibody for 5TGM1 cells) (Research Diagnostics, Fitzgerald Industries).

2. Aspirate the capture antibody and wash three times in PBS/0.05% tween 20 before blocking in PBS/3% BSA for 3 h at room temperature.

3. Serially dilute recombinant mouse IgG2bκ in 1:5 in PBS/0.3% BSA and generate an 8-point standard curve of 500, 100, 20, 4, 0.8, 0.16, 0.032 and 0 ng ml^{-1}.

4. Dilute 1:20 000 for baseline, week 1, 2, 3 and end point sera.

5. Aspirate the blocking solution and wash the plate two times with PBS/0.05% tween 20.

6. Transfer standards and diluted test samples to the plate at 100 μl per well and incubate at 37 °C for 1 h.

7. Dilute detection antibody (provided by Dr Oyajobi, University of Texas, San Antonio, TX, USA) 1:5000 in PBS/0.3% BSA 30 min to 1 h before use.

8. At the end of incubation time, aspirate standards and test samples and wash the plate six times with PBS/0.05% tween 20.

9. Add 100 μl of diluted detection antibody to each well of the plate and incubate at 37 °C for 1 h.

10. Aspirate the detection antibody and wash six times with PBS/0.05% tween 20.

11. Make up the substrate reagent for detection O-phenylene-diamine with 0.05% H_2O_2 (Sigma-Aldrich, St Louis, MO, USA) in H_2O and add 100 μl to each well of the plate and incubate at room temperature.

12. Upon color development (∼15 min), read ELISA plates at 450 nm optical density using a plate reader.

Assessment of myeloma bone disease by microCT

1. Fix hind legs from *in vivo* studies in 10% neutral-buffered formalin (Thermo Scientific); remove muscle attached to hind legs.

2. Scan the bones at an isotropic voxel size of 12 μm using a microCT40 (SCANCO Medical, Bassersdorf, Switzerland) or similar equipment.

3. Trabecular bone measurements are calculated following standard bone analysis protocols.

4. For analysis of cortical bone lesions, export cross-sectional images of the entire metaphysis including the cortices and extending 0.25 mm from the growth plate in tiff format. Then, import the images into AMIRA 3-D graphics software (Mercury Computer Systems, Chelmsford, MA, USA) or similar software. AMIRA software generates a 3-D reconstruction of the metaphyses using a consistent threshold.

5. Count the number of osteolytic lesions that completely penetrate the cortical bone seen in the virtual reconstruction.

Assessment of myeloma bone disease by histology

1. Fix hind legs and spleens in 10% neutral-buffered formalin (Thermo Scientific) for a minimum period of 48 h.

2. Place bones in histological cassettes and decalcify in 10% EDTA in distilled water (pH 7.2) for 2 weeks.

3. Process decalcified bones in the tissue processor (Leica Microsystems, Buffalo Grove, IL, USA) through a dehydration procedure in graded ethanol for two changes of 1 h each in 70% and 95% ethanol, three changes of 1 h each in 100% ethanol and xylene and two changes of 1 h each in paraffin wax at 60 °C.

4. Take the tissues out of the second change of paraffin wax and immerse in a small amount of hot 60 °C paraffin wax with cassettes and cool on a cold plate (Leica Microsystems) to set.

5. Section paraffin-embedded bones and spleens at 5 μm thickness for further analysis using appropriate staining of interest.

Hematoxylin and eosin staining

1. Dewax tissue sections in clearene for 2 × 5 min (Leica Microsystems) and rehydrate through graded ethanol for
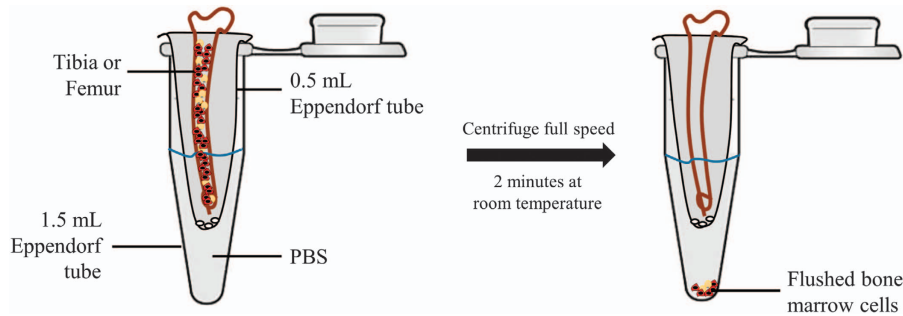
Figure 1 Flushing of bone marrow by centrifugation. Remove lid from 0.5 ml eppendorf tube and puncture the base of the eppendorf tube with a 27-gauge needle. Place this microtube in a 1.5 ml centrifuge tube on ice with 500 μl of PBS. Dissect long bones, removing fat and muscles, and place both tibia and femur in the 0.5 ml eppendorf tube, with open ends at the bottom of the tube. Isolate bone marrow by centrifuging at full speed (13 000 r.p.m.) for 2 min. Wash bone marrow lysates with PBS.

2 min each in 2 × 100%, 2 × 95% and 1 × 70% ethanol and 1 × distilled water.

2. Immerse the slides in working Harris Hematoxylin solution (Thermo Scientific) for 1 min.
3. Rinse slides thoroughly in tap water and enhance the nuclear stain by dipping the sections in 5% ammonium water for 10 s (Thermo Scientific).
4. Counterstain tissue sections with eosin working solution with 2% orange G (Sigma-Aldrich) for 2 min.
5. Finally, rinse sections through graded ethanol, with two changes of clearene, and coverslip using DPX mountant (Sigma-Aldrich).

TRAP staining

1. Dewax tissue sections in clearene and rehydrate through graded ethanol and distilled water as described in hematoxylin and eosin staining section.
2. Incubate the slides in a tartrate/napthol AS-BI phosphate substrate solution pH 5 (Sigma-Aldrich) at 42 °C for 30 min.
3. Immediately after the incubation period, transfer slides to a pararosaniline/nitrite color reaction solution (Sigma-Aldrich) for 10 min at room temperature.
4. Thoroughly rinse the slides in distilled water and counterstain with Harris Hematoxylin solution for 1 min (Thermo Scientific), rinse through graded ethanol, with two changes of clearene, and coverslip using DPX mountant.
5. Alternative to TRAP staining: CTX and ICTP fragments can be measured in plasma, serum and/or urine of myeloma-bearing mice using corresponding assays to assess osteoclast activity.[14]

Mouse Model Selection

Preclinical murine models of multiple myeloma include immunocompetent and immunodeficient mouse myeloma models, xenograft models of human myeloma in mice (in which primary human MM cells can be grown in immunodeficient mice) and genetically engineered models, which attempt to recreate the driver mutations responsible for the development of myeloma from MGUS (**Table 1**). Each system has unique strengths and weaknesses, which must be evaluated in the context of the research question to be addressed.

The immunocompetent 5TMM (5T Radl) model

The 5T murine model of multiple myeloma is based on the discovery by Radl *et al.*[15,16] that a small proportion of aging,

inbred C57BL/KaLwRij mice, an immunocompetent line, spontaneously develop a variety of B-cell proliferative disorders, including malignant monoclonal gammopathies such as multiple myeloma. Subsequent transplantation of bone marrow cells from animals with myeloma to young syngeneic C57BL/KaLwRij mice resulted in a reproducible murine myeloma model in which many features of human myeloma, including tumor growth within the bone marrow, increase in paraprotein, renal dysfunction and development of lytic bone disease, were recapitulated. Unfortunately, the utility of this model was limited by the variability in the proportion of myeloma cells that engrafted per animal.[17]

From the 5T Radl murine myeloma model, a series of distinct myeloma cell lines were established from different original donor animals: 5T2 and 5T33, as well as 5TGM1, a subsequent subclone of the 5T33 line. Inoculation of each of these cell lines into C57BL/KaLwRij mice resulted in myeloma growth within the bone marrow, increased myeloma-specific serum paraprotein and osteolytic bone disease.[15,18,19] Inoculation of 5T2 cells into C57BL/KaLwRij mice recapitulates features of human myeloma and the associated bone disease within ~3 months; however, these cells do not survive well *in vitro* and can only be reliably maintained by direct passage from mouse to mouse, limiting their utility for *in vivo* studies. 5T33 and 5TGM1 cells, in contrast, can be easily cultured *in vitro*. Marrow replacement with tumor is evident ~4 weeks after inoculation of 5T33 or 5TGM1 cells, with a significant increase in paraprotein detectable after ~2 weeks. 5TGM1 cell inoculation, unlike 5T33, also results in the development of lytic bone lesions. Although this model represents only a single clonal type of murine myeloma, the intact immune system of the 5T Radl model provides a major advantage over other immuno-compromised murine myeloma models. Intriguingly, a recent study has shown that C57BL/KaLwRij mice have a Samsn1 deletion, a finding shared with malignant plasma cells from patients.[20]

5TGM1 cells only grow when inoculated into C57BL/KaLwRij mice and do not grow in the closely related C57BL/6 mice. Changing the host microenvironment, either by co-inoculation of bone marrow stromal cells derived from a myeloma-bearing mouse, or via diet-induced obesity, can allow myeloma development in otherwise non-permissive C57BL/6 mice.[21,22] An additional limitation of the 5T Radl model is that it is difficult to cross with genetically modified murine models, thus limiting the model's utility in modeling specific mechanisms involved in myeloma.

Table 1 Examples of immunocompetent and immunocompromised murine models of MMBD induced by MM cell injection (intratibial or intravenous)

Model	Cell type	Mouse strain		Monoclonal protein produced	Reference
5T Radl	5TGM1 5T33 5T2 (murine)	C57BL/KaLwRij	Immunocompetent	IgG2b (murine)	15,18,19
RAG-2	5TGM1 (murine)	*RAG-2* (C57BL/6 background)	Immunocompromised	IgG2b (murine)	23
Xenograft	ARH-77 (human)	Irradiated SCID	Immunocompromised	IgG (human)	52
	JJN3 (human)	Irradiated SCID	Immunocompromised	κ-light chain (human)	30
	KPM2 (human)	SCID	Immunocompromised	IgG (human)	31
	MM.1.S (human)	SCID or NOD/SCID	Immunocompromised	λ-light chain (human)	29
	Vk12653 and Vk12598 (murine)	C57BL/6	Immunocompetent	IgG (murine)	46,48

Immunocompromised RAG-2 model

The RAG-2 model was developed with the goal of establishing a murine model of myeloma in which the host microenvironment could be genetically modified. *Recombinase-activating gene-2* (*RAG-2*)-immunodeficient mice on a C57BL/6 background have abnormal B- and T-cell development, resulting in a myeloma-permissive environment. Fowler *et al.*[23] demonstrated that inoculation of *RAG-2*-deficient mice with GFP-tagged 5TGM1 myeloma cells resulted in the same features of myeloma seen in the 5T Radl model, within a similar time frame of 4 weeks after inoculation and that, importantly, the *RAG-2*-deficient animals could be bred to genetically modified mice to improve investigators' ability to manipulate the host microenvironment. The immunodeficiency of the *RAG-2*-deficient mice, however, remains a disadvantage as compared with the immuno-competent 5T Radl model, as *RAG-2* findings cannot be directly translated to the human microenvironment in myeloma development.

Xenograft murine myeloma models: SCID and NOD/SCID models

Xenograft models, in which human MM cell lines are injected into immune compromised mice (for example, severe combined immunodeficient (SCID), nude, non obese diabetic (NOD)/SCID, etc.), can be used to establish systemic disease (via intravenous injection of MM cells) or local disease (via subcutaneous or intratibial injections). These models offer the opportunity to evaluate homing of MM cells to the bone marrow[8] and to test the efficacy of therapeutics against human myeloma *in vivo*.[24,25] The utility of xenograft models for the evaluation of myeloma cell interactions within the bone marrow micro-environment, however, is not fully understood, as the myeloma bone marrow microenvironments induced in these animals are not easily translated to humans. A recent study using bioen-gineered nanoparticles capable of targeting bone and deli-vering pharmaceuticals to the bone marrow space demonstrated that pre-treatment of NOD/SCID animals with bone-targeting nanoparticles altered the bone marrow niche, delaying engraftment of luciferase-tagged MM1.S (human) MM cells following intravenous injection. This suggests that NOD/SCID models can be used to modulate MM cell–bone marrow microenvironmental interactions.[26]

Several NOD/SCID myeloma models using intravenous injection of human myeloma cell lines, including JJN3, U266, OPM2, XG1, KMM-1, MM.1S, HuNS1, RPMI-8266 and L363, (some of which have been modified to express a fluorescent tag to aid in assessment of tumor volume) or primary human myeloma cells have been described.[8,27,28] Similarly, successful tumor engraftment has been reported with multiple human

myeloma cell lines and SCID mice pre-treated with sublethal irradiation doses.[28–31] In these models, intravenous injection of xenograft cells results in tumor that involves the bone marrow but is not limited to the marrow space. Consistent development of osteolytic bone lesions without dissemination outside of the bone marrow has been described in NOD/SCID models following intravenous injection of JJN3, OPM2 and U266 cell lines, and bone loss has been described following injection of the RPMI-8226 cell line.[28,32] In contrast, intravenous injection of other human MM cell lines, such as KMM-1, into the irradiated NOD/SCID model can result in diffuse extraskeletal disease involvement with plasma-cell infiltration in the bone marrow, as well as the spleen, lungs and liver.[28,33] The presence of extensive extramedullary tumor in these models can be considered a disadvantage as they model an extremely aggressive transformation of myeloma and may not be representative of the more typical indolent course of many cases of human myeloma. In addition, the majority of human MM cell lines are derived from primary human plasma-cell leukemia samples, which have lost their dependence on the marrow microenvironment and are not representative of the heterogeneity seen in patients.[34] Although models that employ primary human samples avoid this problem, design of these experiments must include consideration of the need for a larger sample size than experiments that use cell lines, due to patient variability.

SCID-Hu and SCID-Rab models. The SCID-Hu and SCID-Rab models address the problem of how to accurately model the human myeloma marrow microenvironment *in vivo* and allow the use of primary myeloma cells isolated from patients with multiple myeloma. The SCID-Hu model requires implantation of human fetal bone tissue into irradiated SCID mice, a practice that has raised ethical concerns, before intravenous injection of primary human myeloma cells or human myeloma cell lines. In this system, both human myeloma cell lines and primary human myeloma cells home to the human but not the murine bone marrow.[35,36] It is important, however, to recognize that fetal bone does not accurately recreate the myeloma micro-environment, as development of myeloma occurs almost exclusively in adults. The SCID-Rab model similarly utilizes subcutaneous implantation of non-murine bone tissue, in this case, rabbit bone, into the flank of a SCID mouse. The SCID-Rab model can reproducibly support the growth of primary myeloma cells in the rabbit marrow microenvironment,[37] produce monoclonal immunoglobulin and induce lytic bone lesions, providing a reliable means for testing the efficacy of drug compounds against human myeloma cells but unfortu-nately not replicating the human myeloma microenvironment.

Although the use of rabbit tissue circumvents the ethical concerns associated with the use of fetal human tissue, the SCID-Hu model has an advantage over SCID-Rab model in that it models a human bone microenvironment as opposed to a rabbit bone marrow microenvironment.

SCID-synth-hu model. Similar to the SCID-Hu and SCID-Rab models, the SCID-synth-hu model provides a system for *in vivo* engraftment of human or murine MM cells. In this model, a synthetic 3-D-bone-like, cylindrical, poly-ε-caprolactone polymeric scaffold coated with mouse or human bone marrow stromal cells is subcutaneously implanted into the flank of a SCID mouse.[38] Successful engraftment of human IL-6 and bone marrow-dependent MM cell lines, primary MM cells and peripheral blood plasma-cell leukemia cells on scaffolds coated with human but not murine bone marrow stromal cells has been demonstrated. Importantly, primary human MM cells can be engrafted to scaffolds coated with their own (autologous) bone marrow stromal cells and demonstrated long-term (3–4 months) survival with detectable human monoclonal protein production in the mouse sera. This model has proven suitable for *in vivo* screening of preclinical MM agents.

Another synthetic bone model uses silk scaffolds to generate tissue-engineered bones (TEBs). TEBs are loaded with MM1.S myeloma cells and then inoculated subcutaneously into nude mice. Dissemination and homing to distant skeletal sites can then be observed by confocal microscopy and immunofluorescence.[39]

Genetically engineered models
Multiple recurrently mutated genes have been implicated in the pathogenesis of myeloma, and significant intraclonal heterogeneity exists within individual patients.[40] As spontaneous development of plasma-cell neoplasms in mice is rare, a number of genetically defined murine myeloma systems have been developed in attempt at modeling these mutations and better replicating the pathogenesis of human MM. These efforts have generally involved targeted oncogene expression in B cells with or without mutations in tumor suppressor genes.

IL-6- and MYC-driven models. IL-6 is a potent growth and survival factor in MM that is predominantly secreted by stromal cells in the myeloma bone marrow microenvironment.[41] IL-6 transgenic BALB/c (C) mice (H2-L^d-IL-6) develop plasmacytomas and demonstrate a t(12;15) translocation involving *c-Myc* in the majority of cases;[42] however, penetrance in this model is incomplete (40% at 12 months). As several transgenics have also been generated to target the t(12;15) translocations identified in plasmacytoma models (termed iMyc$^{E\mu}$ and iMyc$^{C\alpha}$), and which mimic the human *MYC* mutations seen in Burkitt's lymphoma, intercrosses of H2-L^d-IL-6 and iMyc transgenics on BALB/c mice have been generated to create MM models with a shorter latency and a higher penetrance. The resultant double-transgenic animals, referred to as C.IL-6/iMyc, demonstrate 100% penetrance with a latency of 3–6 months and phenotypic consistency.[43] Interestingly, ^{18}F-FDG-PET/CT imaging can be used to monitor tumor progression and response to treatment in this model.[44]

Rearrangements of *MYC* are late progression events in MM that are found in ∼40% of advanced MM tumors and have well-defined roles in a number of tumor types. Early attempts at forcing MYC expression, such as those using the Eμ enhancer, which drives transgene expression throughout the B-cell development (Eμ-*Myc* transgenic model[45]), resulted in the development of pre-germinal center lymphomas early in life. The Vk*MYC model is an immunocompetent, de novo model that takes advantage of the propensity of C57BL/6 mice to develop a monoclonal gammopathy with advanced age.[46] In this model, sporadic activation of an engineered MYC transgene flanked by κ-light-chain regulatory sequences and initiated by somatic hypermutation is introduced into C57BL/6 mice. The resulting disease shares biologic and clinical features with human MM.[47] The majority of Vk*MYC animals have an indolent disease course reminiscent of human MM and with age develop a progressive monoclonal plasma-cell population restricted to and dependent on the bone marrow microenvironment. This model also has readily quantifiable monoclonal immunoglobulin secretion (detectable at 20 weeks of age), immunoglobulin deposition in the kidneys and diffuse osteoporosis, as measured by bone mineral density and microCT analysis of femurs, and has proven useful in screening MM therapeutics.[47,48] Penetrance of the Vk*MYC model, as defined by detectable serum monoclonal protein, is 80% by 50 weeks, whereas monoclonal proteins are detectable in 25% of wild-type mice at this time point.

The indolent disease course and late onset of the Vk*MYC model have been interpreted as both an asset (an example that the disease faithfully models clinical features of human MM) and a weakness. Interestingly, a transplanted Vk*MYC (tVk*MYC) model, in which total bone marrow from a Vk*MYC animal is transplanted into wild-type mice following sublethal irradiation, has been used as a model of relapsed refractory MM, similar to the transformation of MM to a more aggressive phenotype.[46]

Two independent bortezomib-resistant myeloma cell lines, Vk12653 and Vk12598, were generated from aged Vk*MYC animals. Similar to the 5T myeloma cell lines, these cell lines can be transplanted to younger syngeneic mice, allowing myeloma engraftment around 4 weeks after transplantation, but cannot be maintained *in vitro*. In comparison with Vk12653, the Vk12598 cell line has been shown to respond completely to melphalan treatment and to partially respond to doxorubicin. Hence, the establishment of these cell lines has permitted investigation of the efficacy of single and combination therapy *in vivo*.[46,48,49]

The Eμ-xbp-1s model. XBP-1 regulates the unfolded protein response and plasma-cell differentiation, is abundantly expressed in human MM cells and can be induced by IL-6, a cytokine that has a critical role in the development of human plasma-cell neoplasms (described further below). Transgenic C57BL/6 mice with XBP-1 overexpression driven by the Eμ enhancer develop a MGUS-MM model with a shortened life span and phenotypic changes in the skin (epidermal thickening with hyperkeratosis and lymphoplasmacytic infiltrates) similar to those seen in the rare plasma-cell disorder POEMS (polyneuropathy, organomegaly, endocrinopathy, serum monoclonal protein and skin lesions) and kidneys resembling human plasma-cell disorders, by 40 weeks.[50] Lytic bone lesions have also been described in this model. Similar to

the Vk*MYC model, the Eμ-xbp-1s has been criticized for its long latency. In addition, the Eμ-xbp-1s model has a low penetrance, with 60% of transgenic animals developing skin changes (rate of development of renal abnormalities was not reported), although the majority of transgenic mice but not control littermates did develop a monoclonal protein in the serum by 20 weeks.

L-GP130 model

The IL-6/JAK/STAT transduction pathway is well-characterized in MM cell growth and survival. Association of the IL-6/IL-6R complex with GP130, a ubiquitously expressed signal transduction component, is critical for human MM survival and proliferation. The L-GP130 model is a retroviral bone marrow transduction-transplantation MM model that transplants IL-3-dependent BA/F3 cells (pre-B cell) that have been infected with a retrovirus encoding the constitutively activated form of GP130, L-GP130, into lethally irradiated syngeneic recipients.[51] The resultant disease has high penetrance, is transplantable into secondary recipient mice and is characterized by bone marrow infiltration with lytic bone lesions, protein deposition in the kidney and monoclonal gammopathy. In addition, analysis of L-GP130 myeloma demonstrated acquired genomic *Myc* abnormalities.

Choice of Myeloma Cell Lines

Murine and human myeloma cell lines and primary human myeloma cells can be used in preclinical *in vivo* models. Although xenograft models using primary human myeloma cells would seem an obvious choice for studies of both the pathogenesis of human myeloma and evaluation of new therapeutic strategies, it is frequently difficult to obtain adequate numbers of primary patient cells at a single time point. Investigators have reported successful engraftment of multiple well-characterized murine and human myeloma cell lines, including, but not limited to 5T myeloma cells (discussed above), ARH-77 cells (a human lymphoblastoid cell line),[52] the human JJN3 myeloma cell line[29] and IL-6-dependent myeloma cell lines.[30] Choice of cell line is generally dependent on the pace of tumor engraftment, characteristics of the particular tumor type (that is, propensity to develop lytic bone lesions or not) and the type of monoclonal protein that is produced.

Conclusion

This review provides an overview of current preclinical models of myeloma and includes specific methods. At the present time, there is no perfect model for the study of multiple myeloma and the associated bone disease, as human cells cannot be studied in an immunocompetent mouse. Therefore, a thorough understanding of the advantages and disadvantages of each model is required in order for an investigator to make a fully informed decision as to the most appropriate model for each research question.

Conflict of Interest

The authors declare no conflict of interest.

References

1. Galson DL, Silbermann R, Roodman GD. Mechanisms of multiple myeloma bone disease. *Bonekey Rep* 2012; **1**: 135.
2. Roodman GD. Mechanisms of bone metastasis. *N Engl J Med* 2004; **350**: 1655–1664.
3. Kumar SK, Rajkumar SV, Dispenzieri A, Lacy MQ, Hayman SR, Buadi FK *et al.* Improved survival in multiple myeloma and the impact of novel therapies. *Blood* 2008; **111**: 2516–2520.
4. Korde N, Kristinsson SY, Landgren O. Monoclonal gammopathy of undetermined significance (MGUS) and smoldering multiple myeloma (SMM): novel biological insights and development of early treatment strategies. *Blood* 2011; **117**: 5573–5581.
5. Fryer RA, Graham TJ, Smith EM, Walker-Samuel S, Morgan GJ, Robinson SP *et al.* Characterization of a novel mouse model of multiple myeloma and its use in preclinical therapeutic assessment. *PLoS ONE* 2013; **8**: e57641.
6. Edwards CM, Edwards JR, Lwin ST, Esparza J, Oyajobi BO, McCluskey B *et al.* Increasing Wnt signaling in the bone marrow microenvironment inhibits the development of myeloma bone disease and reduces tumor burden in bone *in vivo*. *Blood* 2008; **111**: 2833–2842.
7. LeBlanc R, Catley LP, Hideshima T, Lentzsch S, Mitsiades CS, Mitsiades N *et al.* Proteasome inhibitor PS-341 inhibits human myeloma cell growth *in vivo* and prolongs survival in a murine model. *Cancer Res* 2002; **62**: 4996–5000.
8. Mitsiades CS, Mitsiades NS, Bronson RT, Chauhan D, Munshi N, Treon SP *et al.* Fluorescence imaging of multiple myeloma cells in a clinically relevant SCID/NOD *in vivo* model: biologic and clinical implications. *Cancer Res* 2003; **63**: 6689–6696.
9. Oyajobi BO, Munoz S, Kakonen R, Williams PJ, Gupta A, Wideman CL *et al.* Detection of myeloma in skeleton of mice by whole-body optical fluorescence imaging. *Mol Cancer Ther* 2007; **6**: 1701–1708.
10. van Gaalen SM, Kruyt MC, Geuze RE, de Bruijn JD, Alblas J, Dhert WJ. Use of fluorochrome labels in *in vivo* bone tissue engineering research. *Tissue Eng Part B Rev* 2010; **16**: 209–217.
11. Vignery A, Baron R. Dynamic histomorphometry of alveolar bone remodeling in the adult rat. *Anat Rec* 1980; **196**: 191–200.
12. Corral DA, Amling M, Priemel M, Loyer E, Fuchs S, Ducy P *et al.* Dissociation between bone resorption and bone formation in osteopenic transgenic mice. *Proc Natl Acad Sci USA* 1998; **95**: 13835–13840.
13. Dallas SL, Garrett IR, Oyajobi BO, Dallas MR, Boyce BF, Bauss F *et al.* Ibandronate reduces osteolytic lesions but not tumor burden in a murine model of myeloma bone disease. *Blood* 1999; **93**: 1697–1706.
14. Garnero P, Ferreras M, Karsdal MA, Nicamhlaoibh R, Risteli J, Borel O *et al.* The type I collagen fragments ICTP and CTX reveal distinct enzymatic pathways of bone collagen degradation. *J Bone Miner Res* 2003; **18**: 859–867.
15. Radl J, Croese JW, Zurcher C, Van den Enden-Vieveen MH, de Leeuw AM. Animal model of human disease. Multiple myeloma. *Am J Pathol* 1988; **132**: 593–597.
16. Radl J, Croese JW, Zurcher C, Brondijk RJ, Van Den Enden-Vieveen MHM. Spontaneous multiple myeloma with bone lesions in the aging C57BL/KaLwRij mouse as a natural model of human disease. In: Radl J (ed.). *Topics in Aging Research in Europe* 5. EURAGE: Rijswijk, 1985, p 191.
17. Radl J. Idiopathic paraproteinemia--a consequence of an age-related deficiency in the T immune system. Three-stage development—a hypothesis. *Clin Immunol Immunopathol* 1979; **14**: 251–255.
18. Garrett IR, Dallas S, Radl J, Mundy GR. A murine model of human myeloma bone disease. *Bone* 1997; **20**: 515–520.
19. Manning LS, Berger JD, O'Donoghue HL, Sheridan GN, Claringbold PG, Turner JH. A model of multiple myeloma: culture of 5T33 murine myeloma cells and evaluation of tumorigenicity in the C57BL/KaLwRij mouse. *Br J Cancer* 1992; **66**: 1088–1093.
20. Noll JE, Hewett DR, Williams SA, Vandyke K, Kok C, To LB *et al.* SAMSN1 is a tumor suppressor gene in multiple myeloma. *Neoplasia* 2014; **16**: 572–585.
21. Fowler JA, Mundy GR, Lwin ST, Edwards CM. Bone marrow stromal cells create a permissive microenvironment for myeloma development: a new stromal role for Wnt inhibitor Dkk1. *Cancer Res* 2012; **72**: 2183–2189.
22. Lwin ST, Olechnowicz SW, Fowler JA, Edwards CM. Diet-induced obesity promotes a myeloma-like condition *in vivo*. *Leukemia* 2015; **29**: 507–510.
23. Fowler JA, Mundy GR, Lwin ST, Lynch CC, Edwards CM. A murine model of myeloma that allows genetic manipulation of the host microenvironment. *Dis Model Mech* 2009; **2**: 604–611.
24. Neri P, Tagliaferri P, Di Martino MT, Calimeri T, Amodio N, Bulotta A *et al.* In vivo anti-myeloma activity and modulation of gene expression profile induced by valproic acid, a histone deacetylase inhibitor. *Br J Haematol* 2008; **143**: 520–531.
25. Chauhan D, Hideshima T, Anderson KC. A novel proteasome inhibitor NPI-0052 as an anticancer therapy. *Br J Cancer* 2006; **95**: 961–965.
26. Swami A, Reagan MR, Basto P, Mishima Y, Kamaly N, Glavey S *et al.* Engineered nanomedicine for myeloma and bone microenvironment targeting. *Proc Natl Acad Sci USA* 2014; **111**: 10287–10292.

27. Mitsiades CS, Mitsiades N. CC-5013 (Celgene). *Curr Opin Investig Drug* 2004; **5**: 635–647.
28. Paton-Hough J, Chantry AD, Lawson MA. A review of current murine models of multiple myeloma used to assess the efficacy of therapeutic agents on tumour growth and bone disease. *Bone* 2015; **77**: 57–68.
29. Hjorth-Hansen H, Seifert MF, Borset M, Aarset H, Ostlie A, Sundan A *et al.* Marked osteoblastopenia and reduced bone formation in a model of multiple myeloma bone disease in severe combined immunodeficiency mice. *J Bone Miner Res* 1999; **14**: 256–263.
30. Tsunenari T, Koishihara Y, Nakamura A, Moriya M, Ohkawa H, Goto H *et al.* New xenograft model of multiple myeloma and efficacy of a humanized antibody against human interleukin-6 receptor. *Blood* 1997; **90**: 2437–2444.
31. Torcia M, Lucibello M, Vannier E, Fabiani S, Miliani A, Guidi G *et al.* Modulation of osteoclast-activating factor activity of multiple myeloma bone marrow cells by different interleukin-1 inhibitors. *Exp Hematol* 1996; **24**: 868–874.
32. Lawson MA, Paton-Hough JM, Evans HR, Walker RE, Harris W, Ratnabalan D *et al.* NOD/SCID-GAMMA mice are an ideal strain to assess the efficacy of therapeutic agents used in the treatment of myeloma bone disease. *PLoS ONE* 2015; **10**: e0119546.
33. Dewan MZ, Watanabe M, Terashima K, Aoki M, Sata T, Honda M *et al.* Prompt tumor formation and maintenance of constitutive NF-kappaB activity of multiple myeloma cells in NOD/SCID/gammacnull mice. *Cancer Sci* 2004; **95**: 564–568.
34. Dalton W, Anderson KC. Synopsis of a roundtable on validating novel therapeutics for multiple myeloma. *Clin Cancer Res* 2006; **12**: 6603–6610.
35. Urashima M, Chen BP, Chen S, Pinkus GS, Bronson RT, Dedera DA *et al.* The development of a model for the homing of multiple myeloma cells to human bone marrow. *Blood* 1997; **90**: 754–765.
36. Yaccoby S, Barlogie B, Epstein J. Primary myeloma cells growing in SCID-hu mice: a model for studying the biology and treatment of myeloma and its manifestations. *Blood* 1998; **92**: 2908–2913.
37. Yata K, Yaccoby S. The SCID-rab model: a novel *in vivo* system for primary human myeloma demonstrating growth of CD138-expressing malignant cells. *Leukemia* 2004; **18**: 1891–1897.
38. Calimeri T, Battista E, Conforti F, Neri P, Di Martino MT, Rossi M *et al.* A unique three-dimensional SCID-polymeric scaffold (SCID-synth-hu) model for *in vivo* expansion of human primary multiple myeloma cells. *Leukemia* 2011; **25**: 707–711.
39. Roccaro AM, Sacco A, Maiso P, Azab AK, Tai YT, Reagan M *et al.* BM mesenchymal stromal cell-derived exosomes facilitate multiple myeloma progression. *J Clin Invest* 2013; **123**: 1542–1555.
40. Walker BA, Wardell CP, Melchor L, Brioli A, Johnson DC, Kaiser MF *et al.* Intraclonal heterogeneity is a critical early event in the development of myeloma and precedes the development of clinical symptoms. *Leukemia* 2014; **28**: 384–390.
41. Kuehl WM, Bergsagel PL. Molecular pathogenesis of multiple myeloma and its premalignant precursor. *J Clin Invest* 2012; **122**: 3456–3463.
42. Kovalchuk AL, Kim JS, Park SS, Coleman AE, Ward JM, Morse 3rd HC *et al.* IL-6 transgenic mouse model for extraosseous plasmacytoma. *Proc Natl Acad Sci USA* 2002; **99**: 1509–1514.
43. Rutsch S, Neppalli VT, Shin DM, DuBois W, Morse 3rd HC , Goldschmidt H *et al.* IL-6 and MYC collaborate in plasma cell tumor formation in mice. *Blood* 2010; **115**: 1746–1754.
44. Duncan K, Rosean TR, Tompkins VS, Olivier A, Sompallae R, Zhan F *et al.* F-FDG-PET/CT imaging in an IL-6- and MYC-driven mouse model of human multiple myeloma affords objective evaluation of plasma cell tumor progression and therapeutic response to the proteasome inhibitor ixazomib. *Blood Cancer J* 2013; **3**: e165.
45. Adams JM, Harris AW, Pinkert CA, Corcoran LM, Alexander WS, Cory S *et al.* The c-myc oncogene driven by immunoglobulin enhancers induces lymphoid malignancy in transgenic mice. *Nature* 1985; **318**: 533–538.
46. Chesi M, Matthews GM, Garbitt VM, Palmer SE, Shortt J, Lefebure M *et al.* Drug response in a genetically engineered mouse model of multiple myeloma is predictive of clinical efficacy. *Blood* 2012; **120**: 376–385.
47. Chesi M, Robbiani DF, Sebag M, Chng WJ, Affer M, Tiedemann R *et al.* AID-dependent activation of a MYC transgene induces multiple myeloma in a conditional mouse model of post-germinal center malignancies. *Cancer Cell* 2008; **13**: 167–180.
48. Matthews GM, Lefebure M, Doyle MA, Shortt J, Ellul J, Chesi M *et al.* Preclinical screening of histone deacetylase inhibitors combined with ABT-737, rhTRAIL/MD5-1 or 5-azacytidine using syngeneic Vk*MYC multiple myeloma. *Cell Death Dis* 2013; **4**: e798.
49. Guillerey C, Ferrari de Andrade L, Vuckovic S, Miles K, Ngiow SF, Yong MC *et al.* Immunosurveillance and therapy of multiple myeloma are CD226 dependent. *J Clin Invest* 2015; **125**: 2904.
50. Carrasco DR, Sukhdeo K, Protopopova M, Sinha R, Enos M, Carrasco DE *et al.* The differentiation and stress response factor XBP-1 drives multiple myeloma pathogenesis. *Cancer Cell* 2007; **11**: 349–360.
51. Dechow T, Steidle S, Gotze KS, Rudelius M, Behnke K, Pechloff K *et al.* GP130 activation induces myeloma and collaborates with MYC. *J Clin Invest* 2014; **124**: 5263–5274.
52. Huang YW, Richardson JA, Tong AW, Zhang BQ, Stone MJ, Vitetta ES. Disseminated growth of a human multiple myeloma cell line in mice with severe combined immunodeficiency disease. *Cancer Res* 1993; **53**: 1392–1396.